Structural and Spectroscopic Properties of Antiferromagnetically Coupled $Fe^{III}Mn^{II}$ and $Fe^{II}Mn^{II}$ Complexes

Theodore R. Holman, Zhigang Wang, Michael P. Hendrich, and Lawrence Que, Jr.*

Department of Chemistry, University of Minnesota, Minneapolis, Minnesota 55455

Received August 19, 1994[⊗]

The heterobimetallic complexes $[Fe^{III}Mn^{II}BPMP(O_2CCH_2CH_3)_2](BPh_4)_2$ (**1**), $[Fe^{III}Mn^{II}BPMP(O_2CCH_3)_2](BPh_4)_2$ (**1′**), and $[Fe^{II}Mn^{II}BPMP(O_2CCH_2CH_3)_2](BPh_4)$ (**2**), in which BPMP is the anion of 2,6-bis[(bis(2-pyridylmethyl)-amino)methyl]-4-methylphenol, were synthesized and characterized by proton NMR, EPR, and magnetization measurements. The high-spin Fe(III) ($S = {}^5/_2$) and high-spin Mn(II) centers ($S = {}^5/_2$) in **1** and **1′** are antiferromagnetically coupled, resulting in an $S = 0$ ground state in these complexes. Variable temperature magnetic susceptibility measurements show that $J = 23$ cm^{-1} for **1′** ($H = JS_1 \cdot S_2$). The solid state structure of the $Fe^{II}Mn^{II}$ complex (**2**) was determined by X-ray crystallography. Complex **2** crystallizes in the triclinic space group $P\bar{1}$ with the following unit cell parameters: $a = 12.613(6)$ Å, $b = 15.037(13)$ Å, $c = 16.62(2)$ Å, $\alpha = 82.070(5)°$, $\beta = 81.180(5)°$, $\gamma = 67.940(5)°$, and $Z = 2$. Its structure contains a (μ-phenoxo)bis(μ-carboxylato)dimetal cluster with an iron−manganese distance of 3.360(4) Å. Complex **2** is remarkably rich in spectroscopic characteristics. The high-spin Fe(II) ($S = 2$) and high-spin Mn(II) ($S = {}^5/_2$) ions are antiferromagnetically coupled affording an $S = {}^1/_2$ ground state and an unusual EPR signal at 2.5 K. This resonance is broad with $g_{av} < 2$ and exhibits hyperfine features due to the nuclear spin of the Mn(II) ion ($I = {}^5/_2$). At temperatures above 10 K, a second resonance signal appears at $g = 5.8$ which is ascribed to a doublet within the first excited $S = {}^3/_2$ manifold. Variable temperature studies of both the ground and excited state EPR signals have yielded values of $J = 8$ cm^{-1} and $|D_{Fe}| = 5$ cm^{-1}, which approximately agree with the multifield, variable temperature magnetic susceptibility data on the polycrystalline material.

The study of metal−metal interactions has elicited the interest of a broad range of inorganic chemists. Our efforts in this area have been stimulated by the emergence of metalloproteins with carboxylate-bridged bimetallic active sites.[1] In general, such proteins have homodinuclear active sites involving first row transition metals like Fe (hemerythrin,[2] ribonucleotide reducatase,[3] methane monooxygenase,[4] purple acid phosphatase[5]), Co (methionine aminopeptidase),[6] and Zn (alkaline phosphatase,[7a] Klenow fragment of DNA polymerase[7b]). A heterobimetallic $Fe^{III}Zn^{II}$ active site has been found for the purple acid phosphatase from kidney bean,[8] and the related diiron phosphatases from bovine spleen and porcine uterus can be converted into $Fe^{III}M^{II}$ forms by metal substitution.[9] The $Fe^{III}Co^{II}$ form of the porcine enzyme, in particular, has sufficiently altered electronic properties for the bimetallic site as to allow the observation of NOESY cross peaks relating a number of the paramagnetically shifted NMR resonances.[9c]

The ability of the dinucleating ligand H-BPMP[10] to form heterobimetallic complexes with iron being one of the metal ions has allowed us to investigate the novel properties of a number of heterobimetallic complexes.[11−13] The $Fe^{III}Ni^{II}$ complex was the first example of a coupled dinuclear complex wherein EPR signals from both ground and excited spin states were observed.[12] Indeed the temperature dependence of the excited state EPR signal provided an estimate of the antiferromagnetic coupling constant which was corroborated by a variable temperature magnetic susceptibility study. Several Fe^{III}-Cu^{II} derivatives were synthesized, all of which were shown to exhibit low field integer spin EPR signals.[13] One of these provided a test for the spin quantitation protocol developed for complexes with integer spin.[13b] In this paper, we explore the effects of replacing Fe(III) with Mn(II) in a dinuclear BPMP complex to afford an $Fe^{II}Mn^{II}$ complex which is isoelectronic to the $Fe^{III}Fe^{II}$ center. We report the synthesis and properties of the heterobimetallic complexes $[Fe^{III}Mn^{II}BPMP(O_2CCH_2CH_3)_2]^+$ (**1**), $[Fe^{III}Mn^{II}BPMP(O_2CCH_3)_2]^+$ (**1′**), and $[Fe^{II}Mn^{II}BPMP(O_2CCH_2CH_3)_2]^+$ (**2**).

[⊗] Abstract published in *Advance ACS Abstracts,* December 1, 1994.

(1) (a) Karlin, K. D. *Science* **1993**, *261*, 701−708. (b) Que, L., Jr.; True, A. E. *Prog. Inorg. Chem.* **1990**, *38*, 97−200.
(2) (a) Holmes, M. A.; Stenkamp, R. E. *J. Mol. Biol.* **1991**, *220*, 723−737. (b) Holmes, M. A.; Trong, I. L.; Turley, S.; Sieker, L. C.; Stenkamp, R. E. *J. Mol. Biol.* **1991**, *218*, 583−593.
(3) (a) Nordlund, P.; Eklund, H. *J. Mol. Biol.* **1993**, *232*, 123−164. (b) Atta, M.; Nordlund, P.; Åberg, A.; Eklund, H.; Fontecave, M. *J. Biol. Chem.* **1992**, *267*, 20682−20688.
(4) Rosenzweig, A. C.; Frederick, C. A.; Lippard, S. J.; Nordlund, P. *Nature* **1993**, *366*, 537−543.
(5) True, A. E.; Scarrow, R. C.; Randall, C. R.; Holz, R. C.; Que, L., Jr. *J. Am. Chem. Soc.* **1993**, *115*, 4246−4255.
(6) Roderick, S. L.; Matthews, B. W. *Biochemistry* **1993**, *32*, 3907−3912.
(7) (a) Kim, E. E.; Wyckoff, H. W. *J. Mol. Biol.* **1991**, *218*, 449. (b) Beese, L. S.; Steitz, T. A. *EMBO J.* **1991**, *10*, 25−33.
(8) Beck, J. L.; McConachie, L. A.; Summors, A. C.; Arnold, W. N.; de Jersey, J.; Zerner, B. *Biochim. Biophys. Acta* **1986**, *869*, 61−68.
(9) (a) Beck, J. L.; Keough, D. T.; de Jersey, J.; Zerner, B. *Biochim. Biophys. Acta* **1984**, *791*, 357−363. (b) Davis, J. C.; Averill, B. A. *Proc. Natl. Acad. Sci. U.S.A.* **1982**, *79*, 4623−4627. (c) David, S. S.; Que, L., Jr. *J. Am. Chem. Soc.* **1990**, *112*, 6455−6463. (c) Holz, R. C.; Que, L., Jr.; Ming, L.-J. *J. Am. Chem. Soc.* **1992**, *114*, 4434−4436.
(10) Abbreviations used: H-BPMP, 2,6-bis[(bis(2-pyridylmethyl)amino)-methyl]-4−methylphenol; H-BIMP, 2,6-bis[(bis((1-methylimidazol-2-yl)methyl)amino)methyl]-4-methylphenol; TACN, 1,4,7-triazacyclononane.
(11) Borovik, A. S.; Papaefthymiou, V.; Taylor, L. F.; Anderson, O. P.; Que, L., Jr. *J. Am. Chem. Soc.* **1989**, *111*, 6183−6195.
(12) Holman, T. R.; Juarez-Garcia, C.; Hendrich, M. P.; Que, L., Jr.; Münck, E. *J. Am. Chem. Soc.* **1990**, 112, 7611−7618.
(13) (a) Holman, T. R.; Andersen, K. A.; Anderson, O. P.; Hendrich, M. P.; Juarez-Garcia, C.; Münck, E.; Que, L., Jr. *Angew. Chem., Intl. Ed. Engl.* **1990**, *29*, 921−923. (b) Juarez-Garcia, C.; Hendrich, M. P.; Holman, T. R.; Que, L.; Münck, E. *J. Am. Chem. Soc.* **1991**, *113*, 518−525.

0020-1669/95/1334-0134$09.00/0

Experimental Section

All reagents and solvents were purchased from commercial sources and used as received unless noted otherwise. Microanalysis were performed by Desert Analytics, Inc., Tuscon, AZ, while the metal analyses were performed by the Soil Research Laboratory at the University of Minnesota, St. Paul, MN. The solvents CH_2Cl_2 and CH_3CN were distilled from CaH_2 under argon before use. The ligand 2,6-bis[(bis(2-pyridylmethyl)amino)methyl]-4-methylphenol (HBPMP) was synthesized according to published methods.[11,12]

(Bis-μ-*O,O'*-propionato)(2,6-*bis*[(*bis*(2-pyridylmethyl)amino)methyl]-4-methylphenolato)iron(III)manganese(II) Bis(tetraphenylborate), $[Fe^{III}Mn^{II}BPMP(O_2CCH_2CH_3)_2](BPh_4)_2{\cdot}CH_3COCH_3$ (1). $[Fe^{III}Mn^{II}BPMP(O_2CCH_2CH_3)_2](BPh_4)_2{\cdot}CH_3COCH_3$ (**1**) was synthesized according to the following procedures. A solution of 0.1 g (0.19 mmol) of HBPMP in 10 mL of methanol was treated with a solution of 0.076 g (0.19 mmol) of $Fe(NO_3)_3{\cdot}9H_2O$ in 5 mL of methanol to yield a dark blue solution, which contained the mononuclear iron complex. After sequential addition of 47 μL (0.19 mmol) of $Mn(NO_3)_2{\cdot}xH_2O$ (4 M aqueous solution) and 0.055 g (0.57 mmol) of sodium propionate in 5 mL of methanol, the solution was allowed to stir overnight.[14] Subsequently, the addition of a methanolic solution of sodium tetraphenylborate (0.27 g, 0.76 mmol) afforded the solid product, which was filtered through a medium-fritted glass filter. Further purification was achieved by recrystallization of the crude product by vapor diffusion of methanol into an acetone solution of complex (~75% yield). These crystals were diffraction quality and contained one molecule of occluded acetone. Anal. Calcd for $C_{90}H_{89}B_2FeMnN_6O_6$: C, 72.89; H, 6.05; N, 5.67. Found: C, 72.87; H, 5.90; N, 5.87. H NMR, δ (CD_3CN): −9.1 (s), −7.9 (s), 37 (br), 56 (br), 67 (br), 75 (br). IR, COO region: ν_{as}, 1604 cm^{-1}; ν_s, 1426 cm^{-1}.

(Bis-μ-*O,O'*-acetato)(2,6-*bis*[(*bis*(2-pyridylmethyl)amino)methyl]-4-methylphenolato)iron(III)manganese(II) Bis(tetraphenylborate), $[Fe^{III}Mn^{II}BPMP(O_2CCH_3)_2](BPh_4)_2{\cdot}CH_3COCH_3$ (1'). This complex was prepared by using the same experimental procedures outlined for **1** except that $Mn(NO_3)_2$ and $NaO_2CC_2H_5$ were replaced by 0.046 g of $Mn(O_2CCH_3)_2{\cdot}4H_2O$ (75% yield). Anal. Calcd for $C_{88}H_{85}B_2FeMnN_6O_6$: C, 72.64; H, 5.89; N, 5.78; Fe, 3.84; Mn, 3.78. Found, C, 72.83; H, 6.01; N, 5.97; Fe, 3.92; Mn, 3.71. UV−vis (acetone): λ_{max} 385 nm (sh), 596 nm (ϵ = 980 M^{-1} cm^{-1}).

(Bis-μ-*O,O'*-propionato)(2,6-*bis*[(*bis*(2-pyridylmethyl)amino)methyl]-4-methylphenolato)iron(II)manganese(II) Tetraphenylborate, $[Fe^{II}Mn^{II}BPMP(O_2CCH_2CH_3)_2]BPh_4{\cdot}0.8CH_2Cl_2$ (2). $[Fe^{II}Mn^{II}BPMP(O_2CCH_2CH_3)_2]BPh_4{\cdot}0.8CH_2Cl_2$ (**2**) was then prepared by adding 1.1 equiv. of cobaltocene to a solution of complex **1** (0.03 g, 0.019 mmol) in 3 mL of CH_3CN under anaerobic conditions.[15] The purple solution rapidly changed to yellow orange in color, indicating that reduction of the complex had occurred. Upon standing, a yellow precipitate appeared; this was filtered, washed with methanol, and recrystallized from CH_2Cl_2/CH_3CN to yield light orange crystals (0.012 g, 52% yield). Anal. Calcd for $C_{63.8}H_{64.6}B_2Cl_{1.6}FeMnN_6O_5$: C, 65.02; H, 5.50; Fe, 4.76; Mn, 4.68; N, 7.16. Found: C, 65.44; H, 5.77; Fe, 4.69; Mn, 4.29; N, 7.31. UV−vis (acetone): λ_{max} 435 nm, (ϵ = 1200 M^{-1} cm^{-1}).

Crystallographic Studies for $[Fe^{II}Mn^{II}BPMP(O_2CC_2CH_3)_2]BPh_4{\cdot}0.8CH_2Cl_2$ (2). A crystal of **2** (dimensions 0.60 × 0.50 × 0.25 mm) suitable for X−ray diffraction studies was mounted on an Enraf−Nonius CAD4 diffractometer. Crystal data are listed in Table 1, while the details of the diffraction experiment and subsequent calculations can be found in the supplementary material. The cell dimensions were obtained by least-squares refinement of the setting angles for 24 reflections (2θ = 22.4−42°). The stability of the crystal was monitored during the data collection by measuring the intensities of three control reflections after every 4000 s of exposure time. No significant trend in these intensities was observed during the course of data acquisition. Lorentz and polarization corrections were applied to the data, and absorption corrections based on ψ scans were carried out (correction factors 0.87−1.14) using the program, DIFABS.[16]

Table 1. Crystallographic Experiments and Computations for **2**

formula	$C_{64}H_{65}BCl_2FeMnN_6O_5$	fw	1190.76
a, Å	12.613(6)	space group	$P\bar{1}$
b, Å	15.037(13)	temp, K	175
c, Å	16.62(2)	λ, Å	0.7107
α, deg	82.070(5)	D(calc), g cm^{-3}	1.375
β, deg	81.180(5)	μ, cm^{-1}	6.10
γ, deg	67.940(5)	R [a]	0.068
V, Å^3	2876(5)	R [a]	0.072
Z	2		

[a] $R = (\Sigma||F_o| - |F_c||)/(\Sigma|F_o|)$; $R_w = \{(\Sigma\, w|F_o - F_c|^2)/(\Sigma\, w(F_o)^2)\}^{1/2}$.

The structure was solved by using Patterson and Fourier methods using 10087 ($I > \sigma(I)$) out of 10288 reflections. Neutral atom scattering factors (including anomalous scattering) were used.[17] All non-H atoms were refined with anisotropic thermal parameters. Hydrogen atoms were included in calculated positions (C−H = 0.95 Å, $B_H = 1.2\ B_A$, where B_A = isotropic equivalent thermal parameter for the atom to which the proton is attached). Weighted ($w = [\delta^2(R) + gF^2]^{-1}$) least-squares refinement on F was carried out by alternatively refining the cation or the anions plus solvent molecules until the largest shift/esd ratio was equal to 0.02. In the final ΔF map, the highest peaks were located near the partially occupied CH_2Cl_2 solvate positions. Atomic coordinates for the non-hydrogen atoms and selected bond lengths and angles of compound **2** are listed in Tables 2 and 3, respectively. Complete tables of fractional atomic coordinates, thermal parameters, bond lengths, and bond angles for **2** can be found in the supplementary material.

Physical Methods. 1D and 2D ^1H NMR experiments were performed on a Varian VXR 300 NMR spectrometer. The sample was dissolved in CH_2Cl_2 solvent. The 1D spectra were obtained using a 90° pulse with 16K data points. An inversion−recovery pulse sequence was used to obtain non-selective proton longitudinal relaxation times (T_1) with carrier frequency set at several different positions to ensure the validity of the measurements. A typical magnitude COSY spectrum was obtained by collecting 1024 data points in t_2 and 256 data points in t_1 with a repetition time of <0.1 s. The time for the data collection for a 1-mM sample was about 12 h. A zero-degree shifted sine bell combined with a Gaussian function was applied in both dimensions and zero-filled to 2048 (t_2) × 2048 (t_1) data points prior to Fourier transformation and symmetrization.

EPR spectra were obtained at X-band with a Varian E-109 spectrometer equipped with an Oxford Instruments ESR-10 liquid helium cryostat and a Varian E236 bimodal cavity. Samples were prepared under nitrogen, with all solvents distilled prior to use and degassed by five freeze−pump−thaw cycles. For studies at variable temperature, a calibrated carbon-glass resistor (Lakeshore CGR 1000) was frozen into the sample and the EPR tube was positioned to place the resistor just outside the microwave field at the top end of the cavity. The four leads of the resistor were replaced with fine wire, and the top of the tube was sealed with wax to prevent O_2 accumulation during the course of the experiment.

Magnetization measurements were carried out on 20 mg samples with a Quantum Design SQUID magnetometer. Mercuric tetrakis-(thiocyanato)cobaltate was used as a susceptibility standard. The uncertainty of the temperature was about 0.1 K, and that of the susceptibility, about 115 × 10^{-6} cm^3 mol^{-1}. It follows that the uncertainty of $\chi_m T$ is about 0.035 cm^3 mol^{-1} K. The number of measured points was around 60. The Pascal constant of the ligand was estimated to be 630 × 10^{-6} cm^3 mol^{-1}. The holder used in the experiment was a suspended gelatin capsule; its paramagnetism was negligible and its diamagnetism subtracted from the raw data. The fit of the temperature dependence data for **2** required the inclusion of zero-

(14) Unlike in the synthesis of other heterodinuclear complexes, a large amount of $[Fe^{III}Fe^{II}BPMP(O_2CCH_2CH_3)_2]^{2+}$ arose as an impurity if the sample was not allowed to stir overnight.

(15) The direct synthesis of **2** with one mole of Fe^{II} and one mole of Mn^{II} produces a mixture of homo- and heterobimetallic species because the ligand does not differentiate between the two ions and the metals easily undergo intermolecular rearrangement, producing the corresponding homobimetallic species. The current method is more effective because the starting material, $Fe^{III}Mn^{II}$ complex, is pure at the beginning and since the reduced product precipitates rapidly from solution, so the time available for metal rearrangement is minimized.

(16) Walker, S. *Acta Crystallogr.* **1983**, *A39*, 158−166.

(17) *International Tables for X-ray Crystallography;* Kynoch Press: Birmingham, England, 1969; Vol. IV, pp 55, 99, 149.

Table 2. Atomic Coordinates for the Non−Hydrogen Atoms of the Cation of **2** [a]

atom	*x*	*y*	*z*	*B*(eq), Å^2
Fe1	0.18760(8)	0.04010(6)	0.11586(6)	2.39(7)
Mn1	0.1876	0.0401	0.1159	2.4
Fe2	0.14636(7)	−0.10095(6)	0.28358(6)	2.25(6)
Mn2	0.1464	−0.1009	0.2836	2.3
O1	0.2268(3)	−0.0049(3)	0.2350(2)	2.1(3)
O2	0.2059(4)	−0.0845(3)	0.0687(3)	3.8(4)
O3	0.0073(4)	0.0886(3)	0.1609(3)	3.8(4)
O4	−0.0169(4)	−0.0311(3)	0.2471(3)	3.4(3)
O5	0.2214(4)	−0.1851(3)	0.1812(3)	3.8(4)
N1	0.2018(4)	0.1817(3)	0.1348(3)	2.2(4)
N2	0.3783(4)	0.0124(3)	0.0910(3)	2.4(4)
N3	0.1222(4)	0.1356(3)	0.0080(3)	2.5(4)
N4	0.2963(4)	−0.1710(3)	0.3612(3)	2.0(3)
N5	0.0946(4)	−0.0112(3)	0.3931(3)	2.1(3)
N6	0.1232(4)	−0.2337(3)	0.3433(3)	2.3(4)
C1	0.2919(5)	0.0242(4)	0.2736(3)	1.9(4)
C2	0.2751(5)	0.1219(4)	0.2705(3)	2.0(4)
C3	0.3431(5)	0.1502(4)	0.3121(4)	2.4(4)
C4	0.4289(5)	0.0843(4)	0.3559(4)	2.5(4)
C5	0.4444(5)	−0.0125(4)	0.3578(4)	2.3(4)
C6	0.3790(5)	−0.0429(4)	0.3174(4)	2.0(4)
C7	0.1834(5)	0.1941(4)	0.2238(4)	2.5(4)
C8	0.3140(6)	0.1841(5)	0.0983(4)	2.8(5)
C9	0.4079(6)	0.0857(4)	0.1052(3)	2.6(5)
C10	0.5176(6)	0.0714(5)	0.1225(4)	3.3(5)
C11	0.5967(6)	−0.0210(6)	0.1268(4)	4.0(6)
C12	0.5682(6)	−0.0964(5)	0.1137(4)	3.5(5)
C13	0.4583(6)	−0.0766(4)	0.0961(4)	2.9(5)
C14	0.1103(6)	0.2579(4)	0.0927(4)	3.3(5)
C15	0.1002(5)	0.2292(4)	0.0117(4)	2.6(5)
C16	0.0620(6)	0.2952(4)	−0.0530(4)	3.0(5)
C17	0.0425(6)	0.2657(5)	−0.1225(4)	3.5(5)
C18	0.0607(6)	0.1696(5)	−0.1249(4)	3.0(5)
C19	0.1005(5)	0.1072(4)	−0.0583(4)	2.8(5)
C20	0.3983(5)	−0.1485(4)	0.3213(4)	2.1(4)
C21	0.2599(5)	−0.1365(4)	0.4436(4)	2.3(4)
C22	0.0171(5)	0.0787(4)	0.3918(4)	2.4(4)
C23	0.0203(5)	0.1473(4)	0.4364(4)	2.6(4)
C24	0.1062(6)	0.1238(4)	0.4855(4)	2.9(5)
C25	0.1856(5)	0.0313(4)	0.4890(4)	2.6(1)
C26	0.1782(5)	−0.0340(4)	0.4419(4)	2.1(1)
C27	0.3220(5)	−0.2751(4)	0.3651(4)	2.5(1)
C28	0.2134(5)	−0.2977(4)	0.3790(4)	2.3(1)
C29	0.2088(5)	−0.3815(4)	0.4225(4)	2.9(1)
C30	0.1117(6)	−0.4026(5)	0.4241(4)	3.0(1)
C31	0.0210(5)	−0.3405(4)	0.3856(4)	2.8(1)
C32	0.0295(5)	−0.2570(4)	0.3465(4)	2.6(1)
C33	0.2231(6)	−0.1669(5)	0.1063(5)	3.6(1)
C34	0.249(1)	−0.251(1)	0.0562(8)	7.6(3)
C35	−0.0528(6)	0.0485(5)	0.2035(4)	3.3(1)
C36	−0.1816(7)	0.0980(7)	0.2036(6)	4.9(2)
C37	0.5015(6)	0.1178(5)	0.4018(4)	3.6(1)
C38	0.282(2)	−0.333(2)	0.085(2)	6.4(8)
C38′	0.249(2)	−0.240(2)	−0.010(2)	14(1)
C39	−0.2491(9)	0.0589(7)	0.2608(6)	4.4(3)
C39′	−0.215(4)	0.158(4)	0.173(3)	9(2)

[a] Anisotropically refined atoms are given in the form of the equivalent isotropic displacement parameter defined as $(4/3)[a^2\beta_{11} + b^2\beta_{22} + c^2\beta_{33} + ab(\cos\gamma)\beta_{12} + ac(\cos\beta)\beta_{13} + bc(\cos\alpha)\beta_{23}]$.

field splitting terms for the Fe(II) in the spin Hamiltonian (eq 1) as

$$H = J\mathbf{S}_{Fe}\cdot\mathbf{S}_{Mn} + D_{Fe}(S_z^2 - 2) + E_{Fe}(S_x^2 - S_y^2) + \beta(\mathbf{S}_{Fe}\cdot\mathbf{g}_{Fe} + \mathbf{S}_{Mn}\cdot\mathbf{g}_{Mn})\cdot\mathbf{B} \quad (1)$$

described previously.[18] The saturation magnetization data were fitted using the simplex method to find the spin Hamiltonian parameters yielding the minimum in the standard quality of fit parameter, χ^2. This software is now available from WEB Research, 6716 Samuel Rd., Edina, MN 55439.

Table 3. Selected Bond Lengths (Å) and Angles (deg) for **2** [a]

	a. Bond Lengths		
Fe−O1	2.075(4)	Mn−O1	2.073(1)
Fe−O2	2.051(5)	Mn−O4	2.072(2)
Fe−O3	2.156(5)	Mn−O5	2.143(2)
Fe−N1	2.270(5)	Mn−N4	2.286(2)
Fe−N2	2.263(5)	Mn−N5	2.284(2)
Fe−N3	2.194(5)	Mn−N6	2.203(2)
O1−C1	1.336(6)	O2−C33	1.263(8)
O3−C35	1.224(8)	O4−C35	1.272(8)
O5−C33	1.237(8)	N1−C7	1.489(7)
Fe−Mn	3.360(4)		
	b. Bond Angles		
O1−Fe−O2	103.7(2)	O1−Mn−O4	101.8(2)
O1−Fe−O3	89.1(2)	O1−Mn−O5	90.6(2)
O1−Fe−N1	86.9(2)	O1−Mn−N4	86.1(2)
O1−Fe−N2	82.8(2)	O1−Mn−N5	83.3(2)
O1−Fe−N3	160.2(2)	O1−Mn−N6	159.9(2)
O2−Fe−O3	100.3(2)	O4−Mn−O5	97.6(2)
O2−Fe−N1	163.3(2)	O4−Mn−N4	163.0(2)
O2−Fe−N2	92.8(2)	O4−Mn−N5	90.1(2)
O2−Fe−N3	95.5(2)	O4−Mn−N6	98.1(2)
O3−Fe−N1	92.7(2)	O5−Mn−N4	97.4(2)
O3−Fe−N2	166.0(2)	O5−Mn−N5	171.0(2)
O3−Fe−N3	82.4(2)	O5−Mn−N6	83.8(2)
N1−Fe−N2	75.6(2)	N4−Mn−N5	75.7(2)
N1−Fe−N3	75.7(2)	N4−Mn−N6	75.6(2)
N2−Fe−N3	101.7(2)	N5−Mn−N6	99.8(2)

[a] Estimated standard deviations in the least significant digits are given in parentheses.

Results and Discussion

Properties of the $Fe^{III}Mn^{II}$ Complexes (1 and 1′). Measurements on complex **1** support the notion that it contains the (μ-phenoxo)bis(μ-carboxylato)dimetal core found in similar complexes. X-ray studies of the unit cell show that **1** crystallizes in the triclinic space group $P\bar{1}$ and its dimensions are essentially identical to those of previous $Fe^{III}M^{II}$ complexes of the ligand BPMP[12,13] (a = 13.570(23) Å, b = 13.813(8) Å, c = 25.564(38) Å, α = 77.03(8)°, β = 77.05(13)°, γ = 61.07(10)°, Z = 2, V = 4049 Å); it was thus decided not to pursue a detailed crystallographic study of the complex.

A concentrated solution of **1** (5 mM) is EPR silent at 4 K consistent with an antiferromagnetically coupled $Fe^{III}Mn^{II}$ system. This is confirmed by the temperature dependence of the solid state magnetic susceptibility of **1′** measured between 300 and 5.2 K at 0.5 T. The data shows a gradual decrease of the χT value from 5.7 to 0.04 cm^3 mol^{-1} K, which can be fit using a dinuclear model ($H = J\mathbf{S}_1\cdot\mathbf{S}_2$) and affords a J value of 23 cm^{-1} with a 1% Fe(III) monomer impurity (Figure 1). These results compare closely with previous studies of a similar triply bridged complex, $[Fe^{III}Mn^{II}BIMP(O_2CCH_3)_2](ClO_4)_2$, which exhibits a J of 15.4 cm^{-1}.[21] The NMR spectrum of **1** shows only poorly defined features that are expected for Mn^{II} or Fe^{III} complexes but uninformative.

Solid State Structure of $[Fe^{II}Mn^{II}BPMP(O_2CCH_2CH_3)_2]$-$BPh_4\cdot 0.8CH_2Cl_2$ (2). Complex **2** was readily obtained by reduction of **1** by cobaltocene. A crystallographic study of **2** was pursued for comparison with the three available X-ray structures of complexes of BPMP or like ligands with two

(18) Day, E. P.; Kent, T. A.; Lindahl, P. A.; Münck, E.; Orme-Johnson, W. H.; Roder, H.; Roy, A. *Biophys. J.* **1987**, *52*, 837.
(19) Nelder, J.; Mead, R. *Computer J.* **1965**, *7*, 308−313.
(20) Buchanan, R. M.; Mashuta, M. S.; Richardson, J. F.; Oberausen, K. J.; Hendrickson, D. N.; Webb, R. J.; Nanny, M. A. *Inorg. Chem.* **1990**, *29*, 1299−1301.
(21) (a) Borovik, A. S.; Hendrich, M. P.; Holman, T. R.; Münck, E.; Papaefthymiou, V.; Que, L., Jr.; *J. Am. Chem. Soc.* **1990**, *112*, 6031−6038. (b) Jang, H. G., Hendrich, M. P., Que, L., Jr. *Inorg. Chem.* **1993**, *32*, 911−918.

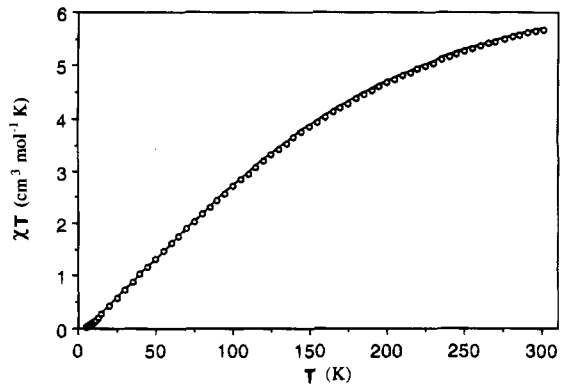

Figure 1. Experimental (○) plot of $\chi_m T$ versus T for a polycrystalline sample of $[Fe^{III}Mn^{II}BPMP(O_2CCH_3)_2](BPh_4)_2$ with the theoretical curve (—) generated from the Hamiltonian $H = JS_{Fe}\cdot S_{Mn} + \beta(S_{Fe}\cdot g_{Fe} + S_{Mn}\cdot g_{Mn})\cdot B$ using $J = 23$ cm^{-1}, $g_{av} = 2.0$ for Fe(III) and Mn(II).

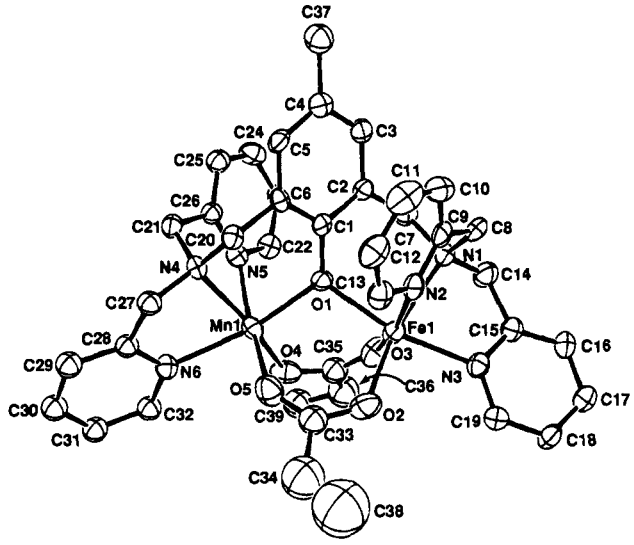

Figure 2. ORTEP plot of the complex cation of **2**, $[Fe^{II}Mn^{II}BPMP(O_2CCH_2CH_3)_2]^+$, with the numbering scheme.

divalent ions: two $Fe^{II}Fe^{II}$ [21] complexes and a $Ni^{II}Ni^{II}$ [22] complex. The structure of **2** (Figure 2) shows an iron and a manganese atom bridged by the phenolate oxygen atom of BPMP and by two additional propionate ligands to form a triply bridged dinuclear core. Most likely, the structural properties are imposed by the requirements of the dinucleating ligand since the $Fe^{II}Mn^{II}$ complex shares many of the features of the related complexes. The phenolate ring plane is rotated relative to the Fe−O−Mn plane, the N(amine)−M−N(pyridine) angles are significantly less than 90°, and the shorter M−O (carboxylate) bonds are trans to the tertiary amine nitrogen atoms. The Fe−Mn separation of 3.360(4) Å is comparable to the value found in the Fe^{II}_2 complex of the same ligand (3.348(2) Å).

Unfortunately, the similar sizes of the ferrous and manganous ions do not allow the two ions to be distinguished in the crystallographic data. In comparison with the corresponding $[Fe^{II}_2BPMP(O_2CCH_2CH_3)_2]BPh_4$ complex,[21a] however, the average bond lengths have increased by about 0.01 Å, which most likely is a consequence of the increase in ionic radius from Fe(II) (0.92 Å) to Mn(II) (0.97 Å).

Properties of the $Fe^{II}Mn^{II}$ Complex 2. The ^{1}H NMR spectrum of **2** shows a number of well-resolved and relatively narrow signals ranging from −20 ppm to 180 ppm in chemical shift (Figure 3). The absence of a 2-fold axis of symmetry

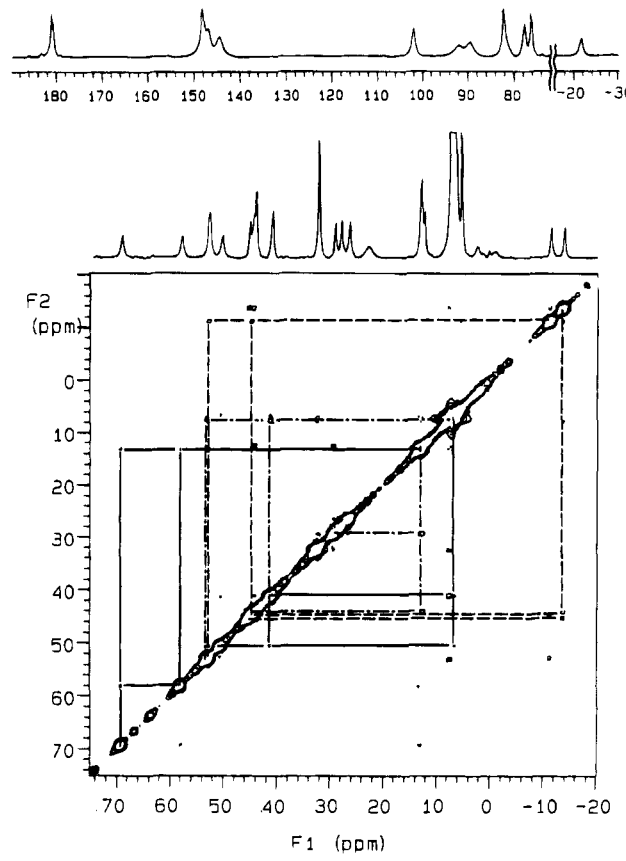

Figure 3. Proton one-dimensional NMR spectrum and homonuclear COSY map of $[Fe^{II}Mn^{II}BPMP(O_2CCH_2CH_3)_2](BPh_4)$ in CD_2Cl_2 at 300 MHz and 20 °C. The COSY spectrum was obtained using 1024 data points in t_2 and 256 data points in t_1 with a repetion time of <0.1 s. A zero-degree shifted sine bell combined with a Gaussian function was applied in both dimensions and zero-filled to 2048 (t_2) x 2048 (t_1) data points prior to Fourier transformation and symmetrization.

should give rise to 37 possible NMR resonances: 16 pyridine protons, three from the meta and para methyl protons on the bridging phenolate ring, six from the α and β protons of the bridging propionates, and 12 from the aminomethylene protons. A total of 33 out of the expected 37 resonances are observed, the pyridyl α protons being too broad to be discerned. This is remarkable considering the presence of a Mn(II) center, whose slow electronic relaxation rate typically obliterates the signals of nearby protons. However, the close proximity of the faster relaxing Fe(II) center and the coupling interaction between the two metal centers give rise to a system spin and a system electronic relaxation rate that engenders the relatively sharp and high resolution spectrum observed.[23]

Specific assignments of these resonances cannot be achieved without selective deuteration or establishing the bond connectivities. Fortunately, the relatively sharp features make 2D NMR studies possible. The ^{1}H COSY spectrum of **2** establishes the bond connectivities in this compound (Figure 3). Fourteen cross peaks are observed in the COSY map within a spectral width of more than 90 ppm, from which the β−γ−β′ connectivities in all the four kinds of pyridyl rings (two cross peaks each) and the α−β connectivities in the two bridging propionates (three cross peaks each) have been established. With the help of the T_1 values, and the data obtained on the $Fe^{II}Fe^{II}$ [21a,24] and $Fe^{II}Zn^{II}$ [21a,25] complexes, the pyridine β and γ protons and the propionate α and β protons were unambiguously assigned

(22) Buchanan, R. M.; Mashuta, M. S.; Oberhausen, K. J.; Richardson, J. F.; Li, Q.; Hendrickson, D. N. *J. Am. Chem. Soc.* **1989**, *111*, 4497−4498.

(23) Bertini, I.; Luchinat, C. *NMR of Paramagnetic Molecules in Biological Systems*; Benjamin Cummings: Menlo Park, CA 1986.

(24) Ming, L.-J.; Jang, H. G.; Que, L., Jr. *Inorg. Chem.* **1992**, *31*, 359−364.

Table 4. NMR Properties of the $Fe^{II}Mn^{II}$ Complex (**2**) with Proposed Assignments[a]

	chemical shift, ppm (T_1, ms)	
	Fe "half"	Mn "half"
BPMP CH_2	181.3 (3.1), 92.2 (0.6), 82.6 (2.9), 23.1 (0.7), 76.6 (3.6), −21.4 (1.8)	148.4 (1.9), 147.5 (1.3), 102.3 (2.1), 144.9 (0.9), 78.1 (2.4), 90.0 (0.7)
pyridine α-H	not observed	not observed
pyridine β-H	53.0 (8.8), 41.3 (*b*), 44.3 (11.3), 29.4 (13.4)	53.0 (8.8), 44.8 (9.2), 45.4 (9.4), 44.3 (11.3)
pyridine γ-H	7.5 (*b*), 12.7 (22.5)	−11.1 (15.9), −13.6 (17.3)
phenolate *m*-H	28.2 (10.8)	26.7 (9.5)
phenolate *p*-CH_3	32.5 (43.0)	
propionate CH_2	50.6 (4.1), 41.3 (4.7)	69.4 (3.7), 58.2 (3.5)
propionate CH_3	6.3 (*b*)	13.3 (6.7)

[a] T_1 values are indicated in parentheses. Assignments are proposed based on chemical shifts, T_1 values, integrations, and bond connectivities (in selected cases). [b] Unable to determine due to overlap.

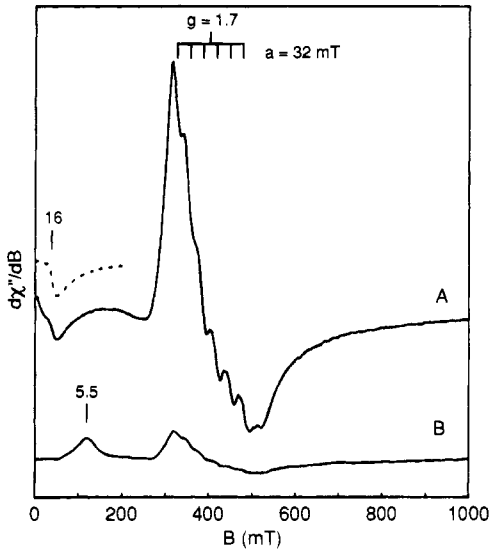

Figure 4. X-Band EPR spectrum of $[Fe^{II}Mn^{II}BPMP(O_2CCH_2CH_3)_2](BPh_4)$ in CH_2Cl_2 at 2.5 K (A) and 10 K (B). Instrumental parameters: microwaves, 0.32 mW at 9.212 GHz; modulation, 1.6 mT at 100 kHz; gain, 3200. A small amount of $[Fe^{II}_2BPMP(O_2CCH_2CH_3)_2](BPh_4)$ is observed at low-field, and a representative spectrum is shown as an insert for comparison (dashed line).

(Figure 3, Table 4). The meta and methyl proton resonances on the bridging phenolate ring were then assigned based on the above results and their T_1 data and integrations (Table 4). Even though the geminal methylene protons are strongly coupled, we did not observe any COSY cross peaks relating the geminal methylene pairs due to their short T_1's. Tentative assignments for the methylene protons were achieved by comparing their T_1 values, which are proportional to the inverse sixth power of the metal−H distance to both ions[23] and by relating them to the corresponding $Fe^{II}Fe^{II}$ and $Fe^{II}Zn^{II}$ complexes.[21a,24,25]

X-band EPR spectra of **2** in CH_2Cl_2 are shown in Figure 4. The T = 2.5 K spectrum (Figure 4A) exhibits two resonances centered at g = 1.7 and 16 ($g = h\nu/\beta B$). The g = 16 resonance is due to a small amount of $Fe^{II}Fe^{II}$ complex arising from disproportionation of **2**.[21b] EPR signals with $g < 2$ are often observed in metal complexes and proteins containing high-spin Fe(III) ($S = {}^5/_2$) and Fe(II) (S = 2) atoms which couple antiferromagnetically to give a system $S = {}^1/_2$ ground state. The presence of a 6-line hyperfine pattern (a = 32 mT) on the g = 1.7 signal indicates that the EPR active center contains a ^{55}Mn nucleus ($I = {}^5/_2$). A similar signal is observed from polycrystalline material. The temperature dependence of the g = 1.7 resonance (intensity·T vs T) is shown in Figure 5; it indicates that the $S = {}^1/_2$ state is lowest in energy. As the temperature is increased, the intensity·T values decrease due to depopulation of the $S = {}^1/_2$ state and population of a low lying $S = {}^3/_2$ excited state. This is also evident in the EPR spectrum with the growth of a new resonance at g = 5.5 (Figure 4B) which arises from a doublet within the $S = {}^3/_2$ state. The temperature dependence of the g = 5.8 signal is shown in Figure 5. All signals broaden due to fast relaxation for $T > 50$ K.

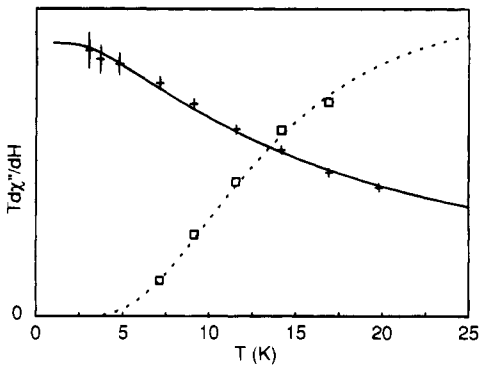

Figure 5. Temperature dependence of the g = 1.7 (+) and 5.5 (□) signals of $[Fe^{II}Mn^{II}BPMP(O_2CCH_2CH_3)_2](BPh_4)$ in CH_2Cl_2. The signal intensities were determined from the zero-to-peak height. The theoretical curves were computed from eq 1 with J = 8 cm^{-1}, D_{Fe} = 5 cm^{-1} for the ground $S = {}^1/_2$ doublet (solid line) and the upper doublet of the S = 3/2 quartet (dashed line). The ordinate scales for both plots are arbitrary.

The temperature dependence of the $S = {}^1/_2$ doublet is dependent on the magnitude of J, but not significantly on the zero-field splitting of the Fe(II) center. Fits to the temperature dependence of this signal based on eq 1 are shown in Figure 5 and give $J = 8 \pm 2$ cm^{-1}. The temperature dependence of the S = 3/2 signal is dependent on both J and D_{Fe}; we neglect D_{Mn} since these values are typically less than 0.1 cm^{-1}. Thus for J = 8 cm^{-1}, the fits to the $S = {}^3/_2$ temperature dependence also shown in Figure 5 give $|D| = 5 \pm 2$ cm^{-1}.

Further details concerning the electronic properties of **2** are still under consideration. Simulations of the $S = {}^1/_2$ EPR spectrum have not been able to reproduce simultaneously both the hyperfine features and the broad tail extending to 1000 mT. In addition, we have not been able to accurately determine the intrinsic hyperfine A-values of the Mn(II) site. This is due to uncertainty regarding the large anisotropy that the Fe(II) site projects onto the system $S = {}^1/_2$ state. For example, with J = 8 cm^{-1} and D = 5 cm^{-1}, the spin expectation values of the Mn(II) site are $\langle \mathbf{S} \rangle = 1.38_x, 1.38_y, 0.70_z$ for $E/D = 0$ or $\langle \mathbf{S} \rangle = 0.84_x, 1.88_y, 0.61_z$ for $E/D = 0.3$. Since the intrinsic A-value, A_{Mn}, is related to the experimentally observed value by $\mathbf{A}_{Mn} = \mathbf{A}_{obs}/2\langle \mathbf{S} \rangle$, the calculation of $\mathbf{A}_{Mn}$ requires a determination of the rhombicity of the Fe(II) site. However, a determination of E/D relies on simulations of the spectra, which are not available. A similar problem exists for dinuclear complexes containing Mn(III) sites such as $[Fe^{II}Fe^{III}O(O_2CCH_3)_2(Me_3TACN)_2]^{2+}$ and $[Mn^{II}Mn^{III}BIMP(O_2CCH_3)_2]^{2+}$, both of which give rise to antiferromagnetically coupled $S = {}^1/_2$ ground states.[26] The reported intrinsic Mn A-values for these complexes may change significantly when the zero-field splittings of the Mn(III) site(s) are taken into account.

Solid state magnetic susceptibility measurements on a polycrystalline solid of **2** also indicate the presence of weak

(25) Wang, Z.; Holman, T. R.; Que, L., Jr. *Magn. Reson. Chem.* **1993**, *31*, S78−S84.

(26) (a) Bossek, U.; Weyhermüller, T.; Wieghardt, K.; Bonvoisin, J.; Girered, J. J. *J. Chem. Soc., Chem. Commun.* **1989**, 633−636. (b) Diril, H.; Chang, H.-R.; Nilges, M. J.; Zhang, X.; Potenza, J. A.; Schugar, H. J.; Isied, S. S.; Hendrickson, D. N. *J. Am. Chem. Soc.* **1989**, *111*, 5102−5114.

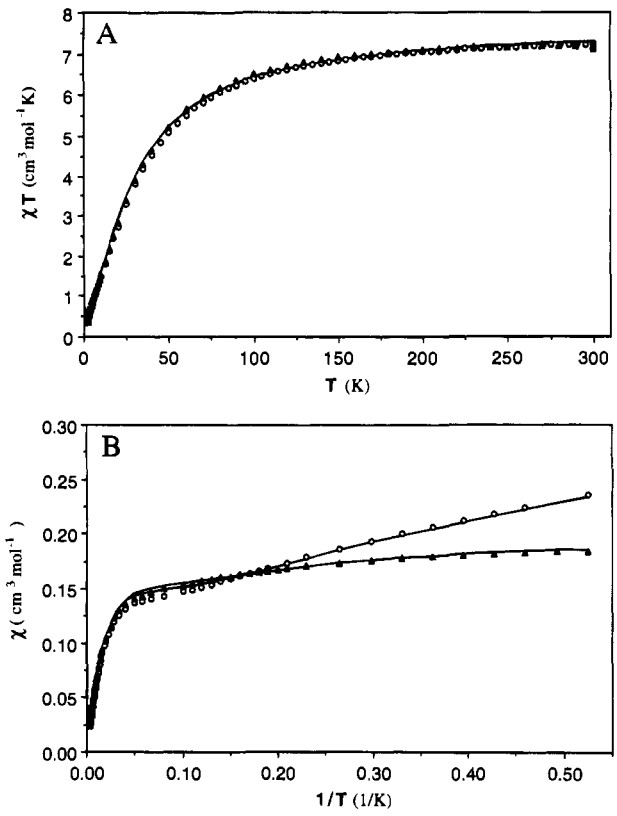

Figure 6. Experimental (○ (0.5 T) and △ (5.0 T)) plots of χT vs T (A) and χ_m versus $1/T$ (B) for a polycrystalline sample of $[Fe^{II}Mn^{II}BPMP(O_2CCH_2CH_3)_2](BPh_4)$ with the theoretical curves (—) generated from eq 1 using $J = 5$ cm^{-1}, $D = 7$ cm^{-1}, $E/D = 0.2$, and $g_{av} = 2.1$ for Fe(II) and $D = 0.0$ cm^{-1}, $E/D = 0.0$, and $g_{av} = 2.0$ for Mn(II).

antiferromagnetic coupling. The χT values decrease from 7.3 to 0.35 cm^{-3} mol^{-1} K, upon changing the temperature from 300 to 1.9 K. Unlike the $Fe^{III}Mn^{II}$ complex, these data could not be simulated with a spin Hamiltonian that ignores zero-field splitting, because the D value of the Fe(II) center is comparable to the exchange coupling. The multiple field data was fit utilizing full diagonalization of the spin Hamiltonian of eq 1. Figure 6 shows plots of χT vs T and χ versus $1/T$ at applied fields of 0.5 and 5.0 T, with the solid lines representing the theoretical curves. The simulations were achieved utilizing the following parameters: $J = 5.0(5)$ cm^{-1} and $|D_{Fe}| = 7(3)$ cm^{-1}. It should be noted that the quality of the fit was very sensitive to the value of J; deviations of greater than 0.5 cm^{-1} produced markedly inferior fits. Variations in the value of D between 4 and 10 cm^{-1}, however, did not affect the fit as greatly. The zero-field parameters for the Mn(II) were set to zero since they are typically much smaller than those of Fe(II) and had little effect on the quality of fit. Because approximately 5% (based on EPR) of the Fe^{II}_2 complex was present in the sample as an impurity, the simulations were performed using data which had the appropriate amount of the Fe^{II}_2 complex subtracted from the original raw data. The corresponding Mn^{II}_2 impurity was not taken into account because the Mn^{II}_2 complex has markedly different solubility properties and does not co-crystallize to any appreciable amount under the conditions presented here.

Conclusions

In this work, the physical and spectroscopic properties of three complexes, $[Fe^{III}Mn^{II}BPMP(O_2CCH_2CH_3)_2](BPh_4)_2$ (**1**), $[Fe^{III}Mn^{II}BPMP(O_2CCH_3)_2](BPh_4)_2$ (**1′**), and $[Fe^{II}Mn^{II}BPMP(O_2CCH_2CH_3)_2]BPh_4$ (**2**) were investigated using a variety of physical and spectroscopic methods. In the $Fe^{III}Mn^{II}$ complexes, the high spin Fe(III) is antiferromagnetically coupled ($J = 23$ cm^{-1}) to the Mn(II) ion resulting in an $S = 0$ ground state which accounts for its featureless ^{1}H NMR spectrum and EPR silence. However, the $Fe^{II}Mn^{II}$ complex exhibits rich spectroscopic features. Due to the antiferromagnetic coupling between the high spin Fe(II) and Mn(II) ions, the NMR spectrum of **2** exhibits a large number of well resolved resonances, despite the presence of Mn(II), whose electronic properties typically afford NMR features that are too broad to observe at high resolution. This effectively illustrates the dramatic ability of one metal ion (Fe(II)) to affect the relaxation properties of another (Mn(II)), via the coupling interaction. EPR is also a powerful probe for understanding metal−metal interactions in **2**. By analysis of the temperature dependence of the ground state and excited state signals, values of J and $|D_{Fe}|$ were both determined. To our knowledge, this is the first example for which both J of a coupled system and D of a ferrous ion have been determined by analysis of the excited state EPR properties.

The exchange coupling of the corresponding homonuclear (μ-phenoxo)Fe^{III}_2 complex is $J = +24$ cm^{-1}.[1b] This value is considerably smaller than that of oxo-bridged complexes presumably because of the shift of electron density away from the oxo exchange pathway toward the phenyl ring. This exchange coupling is close to the value reported here for **1**, as might be expected since both complexes have the same number of unpaired electrons. These antiferromagnetic J-values are greater than that reported for a related complex, $Fe^{III}Mn^{II}$bimp ($J = +15$ cm^{-1}); however, this value may be artificially low owing to the presence of an additional ferromagnetic species, which gives rise to an $S = 5$ EPR spectrum.[20]

Studies on the $Fe^{II}Mn^{II}$ complex may also help in the analysis of the spectroscopic results of (μ-oxo)diiron proteins in their $Fe^{II}Fe^{III}$ and $Fe^{II}Fe^{II}$ oxdiation states. Previous investigations of these proteins and even model compounds have been hampered by the large number of parameters needed to simulate the data. For example, we have attempted to analyze the Mössbauer data of a diiron(II) complex of BPMP; however, the problem includes too many unknown variables (i.e. J, D_1, D_2, E_1/D_1, E_2/D_2, and tensor angles for both metals). The advantage of the $Fe^{II}Mn^{II}$ complex is that it is isoelectronic with the corresponding $Fe^{III}Fe^{II}$ form, and the Mn(II) ion simplifies the Mössbauer analysis since there is only one iron site to probe instead of two as in the diiron systems. In addition, the EPR and magnetic susceptibility mesurements have established approximate values for J and D_{Fe}. Subsequent analysis of the low temperature, high field Mössbauer data may be possible since the number of unknowns has been reduced considerably.

Acknowledgment. We thank Prof. J. D. Britton for his generous help in solving the structure of the $Fe^{II}Mn^{II}$ complex and Dr. E. P. Day for providing expertise and assistance for the susceptibility study. This work has been supported by the National Institutes of Health through grants GM38767 (L.Q.) and GM49970 (M.P.H.). T.R.H. was a recipient of a Doctoral Dissertation Fellowship from the Graduate School of the University of Minnesota.

Supplementary Material Available: X-ray structural information for $[Fe^{II}Mn^{II}BPMP(O_2CCH_2CH_3)_2]BPh_4 \cdot 0.8CH_2Cl_2$ (**2**), including crystallographic data, tables of atomic coordinates, thermal parameters, and intramolecular bond lengths and angles (31 pages). This material is contained in many libraries on microfiche, immediately follows this article in the microfilm version of the journal, and can be ordered from the ACS; see any current masthead page for ordering information.

IC9409874